Cd and In-doping in thin film SnO_2

Juliana Schell,[1,2] Doru C. Lupascu,[2] Artur Wilson Carbonari,[3] Ronaldo Domingues Mansano,[4] Rafael. S. Freitas,[5] João Nuno Gonçalves,[6] Thien Thanh Dang,[7] ISOLDE collaboration[1] and Reiner Vianden[7]
[1]*European Organization for Nuclear Research (CERN), CH-1211 Geneva, Switzerland*
[2]*Institute for Materials Science and Center for Nanointegration, Duisburg-Essen (CENIDE), University of Duisburg-Essen, 45141 Essen, Germany*
[3]*Instituto de Pesquisas Energéticas e Nucleares, Universidade de São Paulo, 05508-000 São Paulo, Brazil*
[4]*Escola Politécnica, Universidade de São Paulo, 05508-010 São Paulo, Brazil*
[5]*Instituto de Física, Universidade de São Paulo, 05314-970 São Paulo, Brazil*
[6]*CICECO—Aveiro Institute of Materials and Departamento de Física, Universidade de Aveiro, 3810-193 Aveiro, Portugal*
[7]*Helmholtz-Institut für Strahlen-und Kernphysik, Universität Bonn, Nussallee 14-16, 53115 Bonn, Germany*

(Received 8 November 2016; accepted 3 May 2017; published online 18 May 2017)

In this paper, we investigate the effects of doping in the local structure of SnO_2 by measuring the hyperfine interactions at impurity nuclei using the Time Differential Perturbed Gamma-Gamma Angular Correlation (TDPAC) method in addition to density functional theory simulations. The hyperfine field parameters have been probed as a function of the temperature in thin film samples. The experimental results reveal that ^{117}Cd/In and ^{111}In/Cd are incorporated and stabilized in the SnO_2 lattice replacing the cationic site. Significant differences in the electric field gradient were observed from TDPAC measurements with both the probe nuclei. Furthermore, the absence of strongly damped spectra further indicates that implanted Cd atoms (for ^{117}Cd/In probe nuclei measurements) easily occupy regular substitutional Sn sites with good stability. The simulated value for the electric field gradient obtained with the first oxygen neighbor removed is closer to the experimental value observed for ^{117}Cd, which also indicates this configuration as stable and present in the sample. *Published by AIP Publishing.* [http://dx.doi.org/10.1063/1.4983669]

INTRODUCTION

Stannic oxide is a semiconductor with a bandgap of $E_g \sim 3.6$ eV, which crystallizes in the rutile structure with a tetragonal lattice and a space group of $P4_2/mnm$. In contrast to other oxides, it has high transparency in the visible range and high electrical conductivity. Furthermore, it also displays good chemical stability with high melting and boiling points and a low production cost. Currently being used as gas sensors, tin (IV) oxides are further applied as humidity sensors, transparent electrodes for solar cells, varistors, optoelectronic devices, capacitors, flat-panel displays, high capacity anodes in lithium-ion batteries, and many other electronic devices.[1–3]

Similar to other semiconductors, defects and small concentrations of impurity dopants change the SnO_2 conductivity by several orders of magnitude, being particularly sensitive to the presence of oxygen vacancies and interstitial Sn.[1] Together with the doping benefits, it is known that +2 valence elements lead to an increased extrinsic defect concentration mediated by oxygen vacancies. Cadmium doping in stannic oxide decreases the resistivity and enhances the performance for sensing molecules, particularly ethanol or H_2,[4] with the sensitivity of H_2S being enhanced by more than 20 times when compared with pure SnO_2.[5] It has been reported that when indium acts as an acceptor dopant, compensating the unintentionally doped electrons, it produces an increase in the resistivity of SnO_2 films.[6] However, experimental investigations in thin films deposited by the sol-gel technique by Sujatha *et al.*[7] show that n-type conductivity is present at In concentrations below 5%.

From the few examples presented above, it is clear that the effectiveness of metal ion doping and manufacturing processes in SnO_2 is quite complex and an atomistic view of the structure may be elucidated. This motivated hyperfine interaction studies already in the late eighties. Desimoni *et al.*[8] studied the incorporation of In from $^{111}InCl_3$ solution while forming SnO_2 from the Sn metal being oxidized during annealing treatments. They reported the signal from a substitutional site for ^{111}In in a sample subjected to intense defect distribution centered at $\omega_Q = 35.6\,(1.8)$ Mrad/s and $\eta = 0.40$ and a minor component characterized by $\omega_Q = 17.2\,(0.6)$ Mrad/s and $\eta = 0.77$ interpreted as small precipitates of In_2O_3. The definitions of ω_0, ν_Q, and η are given below. Renteria *et al.*[9] performed Time Differential Perturbed Gamma-Gamma Angular Correlation (TDPAC) studies on SnO_2 thin films using the ^{111}In/Cd probe identifying two Sn 2^+ and 4^+ oxidation states in different SnO and SnO_2 phases. The hyperfine coupling frequency $\nu_{Q1} = 117(1)$ MHz and $\eta = 0.18(2)$ were assigned to In/Cd in cation lattice sites of SnO_2, in agreement with previous results obtained by Wolf *et al.* in powder samples.[10] Ramos *et al.*[11,12] report two environments of the ^{111}In probe atoms in the thin films and nano-structured powder SnO_2 characterized by hyperfine parameters $\nu_{Q1} = 115$ MHz and $\eta \sim 0.1$, assigned to ^{111}In probe atoms at substitutional Sn sites and $\nu_{Q2} = 146$ MHz and $0{,}4 \leq \eta \leq 1$ assigned to defects and the disordered SnO_2 phase. Muñoz *et al.*[13] performed

TDPAC measurements in SnO pellets after the ^{111}In diffusion, observing one major fraction for Cd in a neutral charge state. The other fraction was also assigned to the cation-site but in the charge state q = +1.

In this paper, the γ-γ TDPAC technique was used to measure hyperfine parameters in SnO_2 thin films, complementing our previous systematic investigation of structural defects due to impurity doping from an atomic point of view.[11,12,14] To our knowledge, no TDPAC measurements in SnO_2 samples using ^{117}Cd have been done before.

TDPAC OBSERVABLES

The charge distribution and magnetic moments around an atom generate electric field gradients, EFGs, and/or magnetic fields, which interact with the electric quadrupole nuclear moments and/or the nuclear magnetic dipole moment of the probe nuclei, leading to the hyperfine interactions. These interactions, which provide an atomic scale insight into the neighboring electronic and atomic environment of the probe atom, can be studied by common techniques like the Mößbauer Effect, Nuclear Magnetic Resonance, and Nuclear Orientation. The advantage of the *less-known* nuclear radioactive Time Differential gamma-gamma Perturbed Angular Correlation technique[15] is that it works for many probe nuclei under ppm concentrations. The signal quality of the TDPAC technique is independent of the measuring temperature, and the measurements are time differential in a nanosecond/microsecond timescale range. Consequently, investigations using the TDPAC technique provide information about electric field gradients and magnetic fields generated by the electronic, ionic, and spin distribution in the vicinity with high precision at any temperature. Therefore, probe sites, their interaction with point defects and phase transitions, the electronic dynamic and diffusion processes, can be studied.

The Hamiltonian of the electric hyperfine interaction can be written in terms of V_{zz} and the asymmetry parameter η in the following form

$$\hat{H}_{el} = \left[\frac{(eQV_{zz})}{4I(2I-1)}\right]\left[3I_z^2 - I(I+1) + \left(\frac{\eta}{2}\right)\left(I_+^2 + I_-^2\right)\right]. \quad (1)$$

If I_+ and I_- are the nuclear angular momentum operators, TDPAC measures the perturbation function $R(t) \approx A_{22}G_{22}(t)$ for different perturbation factors $G_{22}(t)$, as shown in Equations (2) and (3) for spins 3/2 and 5/2, respectively,

$$G_{22}(t) = \frac{1}{5}[1 + 4\cos(\omega_1 t)], \quad (2)$$

$$G_{22}(t) = \sum_{n=0}^{3} s_n(\eta)\cos(\omega_n t). \quad (3)$$

For nuclear spins 3/2 and 5/2, the observable ω_n frequencies are given by $\omega_1 = \omega_0 = 6\omega_Q\sqrt{(1+\eta^2/3)}$ and $\omega_n = 6\omega_Q C_n(\eta)$, respectively. The coefficient C_n can be numerically calculated for a known η.[14] The coefficients s_n denote the amplitudes of the transition frequencies ω_n and are summations of Wigner 3j-symbol products running over the allowed magnetic splitting hyperfine states.[16] The axial asymmetry of the EFG tensor or deviations from it is described by the asymmetry parameter $\eta = (V_{xx} - V_{yy})/V_{zz}$. The major component of the EFG tensor V_{zz} can be obtained from the observable spin dependent quadrupole frequency ω_Q for nuclear spins 3/2 and 5/2 by

$$\omega_Q = \frac{eQV_{zz}}{12\hbar}; \quad \omega_Q = \frac{eQV_{zz}}{40\hbar} \quad (4)$$

with Q being the nuclear quadrupole moment. Further details about the TDPAC technique can be found in Refs. 15 and 16. In this paper, we focus on electric hyperfine interactions since there is no evidence of magnetism involved in our studies. Nuclear quadrupole interactions are extremely sensitive to subtle local distortions and charge polarization because the EFG is determined primarily by the electrons involved in the bonding with the nearest neighbors.

EXPERIMENTAL METHODS

SnO_2 thin films were deposited on Si (1 0 0) p-type wafers using sputtering. A 0.05 T magnetic field was applied to the target 10 cm away from the Si wafer substrate using the processing gases Ar (99.999%) and O (99.998%). The substrate temperature did not exceed 363 K during the deposition, and the thickness of the films was 100 nm. Some TDPAC spectra of the thin film using ^{111}In have been previously published by some of us.[12] We have included the results in the present discussion for comparison. The ^{111}In implantation was performed at 160 keV at Helmholtz-Institut für Strahlen-und Kernphysik (HISKP), in Bonn, for measuring the probing 245 keV state on ^{111}Cd.

The implantation of ^{117}Ag radioactive ion beams was performed at the Isotope Mass Separator On-Line (ISOLDE)[17] at CERN at 30 keV with 10^{11} atoms/cm^2 fluency. The UC_x target was installed at the General Purpose Separator (GPS). The Resonance Ionization Laser Ion Source (RILIS)[18] was used to increase the beam purity and efficiency to 10^8 at/μC. The beam of the short lived ^{117}Ag ($t_{1/2}$ = 73 s) was implanted at the GPS low mass beam line. The fast, high energy β^--decay of ^{117}Ag to ^{117}Cd ($t_{1/2}$ = 2.49 h) imparts a strong recoil of ~21 eV, re-implanting the ^{117}Cd atom before it decays to the probing state on ^{117}In. The daughter nucleus ^{117}In has an excited state at 660 keV with Q = (−)0.59(1) b, $t_{1/2}$ = 53.6 ns, and I = 3/2 being an excellent isotope for TDPAC measurements using the 89–345 keV gamma-ray cascade.[19] Alternatively, ^{111}In ($t_{1/2}$= 2.8 d) decays to ^{111}Cd.[19]

Defects produced during implantation of dopants result from knock-out changes in atomic positions merging together with an increasing concentration of point defects within a small space region. ^{111}In and ^{117}Ag were implanted at incidence angles of 12° and 0°, respectively. The rapid thermal annealing (RTA) process was applied to effectively recover the implantation damage at 873 and 973 K for ^{111}In and ^{117}Ag, respectively.

RESULTS AND DISCUSSION

^{117}Cd(^{117}In): SnO_2 thin film

Fig. 1 shows the R(t) function obtained from TDPAC measurements at room temperature after implantation of

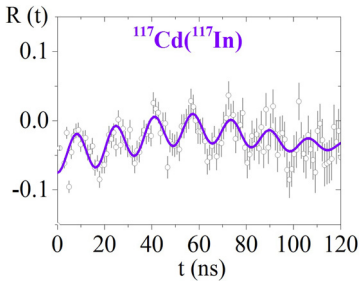

FIG. 1. TDPAC spectrum of the SnO_2 thin film of 100 nm thickness using ^{117}Cd/In and after heat treatment for 5 min in air at 973 K.

^{117}Ag into the SnO_2 thin film with subsequent annealing at 973 K for 5 min in air. The results show evidence that ^{117}In probe nuclei interact with two different local environments as revealed by the two observed frequencies $\omega_{01} = 391.5(5)$ Mrad/s ($|Vzz_1| = 8.7(1) \cdot 10^{21}$ V/m^2) and $\omega_{02} = 50.2(4)$ Mrad/s, respectively, with different fractions of probe nuclei, $f_1 = 57.4$ (1) % and $f_2 = 43.2$ (1) %, interacting with different EFG_1 and EFG_2. Experimental data were fitted with fixed $\eta = 0$ for both EFG.

Since the probe excited state has spin 3/2, in the absence of the magnetic field, there is only one observable frequency and ω_0 and η cannot be separately identified. Therefore, the density functional theory was used with the full potential LAPW + lo method implemented in the WIEN2k code,[20] and with the PAW method[21] implemented in the VASP code,[22] to simulate the electric field gradient parameters at the In probe occupying a Sn substitutional site. The lattice constants were fixed in the experimental values of the pure compound,[23] and all the free fractional atomic coordinates were optimized. A $2 \times 2 \times 3$ supercell ($a = b = 13.40$ Å and $c = 9.56$ Å) of the SnO_2 host was considered, where one of the Sn atoms was replaced by the In impurity. The GGA-PBE approximation for the exchange-correlation functional was used.[24] Table I shows the WIEN2k results for two different types of charge supercells: (1) a neutral In supercell and (2) when doped by one more electron (+1) accounting for In having the same number of shared electrons with the oxygen neighboring atoms as Sn.

In order to check the results with a larger supercell and study the effect of vacancies, we considered a $3 \times 3 \times 3$ supercell. In this case, we used the VASP code with the PAW method, which allowed faster relaxation and convergence. For the case of an impurity substitutional at the Sn site, we obtained $V_{zz} = 6.42 \times 10^{21}$ V m^{-2} and $\eta = 0.52$, which are close to the values found with the smaller supercell by WIEN2k. We conclude that the value converged with respect to the size of the supercell, and the remaining discrepancy may be attributed to limitations of the exchange-correlation functional or to temperature effects not taken into account in this calculation. On the other hand, other configurations including defects such as oxygen vacancies may be favorable, as will be explored next.

TABLE I. Electric field gradient parameters at the In impurity substitutional at the Sn site in a SnO_2 $2 \times 2 \times 3$ supercell.

Doping	V_{zz} (10^{21} V/m^2)	ω_0 (Mrad/s)	η
Neutral	6.87	308	0.24
+1 electron	6.59	295.5	0.34

To study the possible effect of vacancies in the hyperfine parameters of the probe, we started with the previous supercell and additionally removed one oxygen atom. Three independent calculations were considered, where the removed oxygen is the first, second, and third neighbor of the probes. The obtained results are $V_{zz} = -9.49 \times 10^{21}$ V m^{-2} and $\eta = 0.64$; $V_{zz} = 12.28 \times 10^{21}$ V m^{-2} and $\eta = 0.06$; $V_{zz} = 6.42 \times 10^{21}$ V m^{-2} and $\eta = 0.33$, respectively. The removal of the first two oxygen neighbors, in the oxygen octahedron surrounding the impurity, causes an increase in V_{zz} with respect to the result without vacancies, while for the third neighbor with vacancies, the differences are much smaller, but the differences are not very large in any case. Of the three cases, the one with the lowest energy is where the first neighbor is removed (the second neighbor has approximately the same energy, only higher by 16 meV per supercell), but the third one has a larger difference of 0.52 eV. Interestingly, the value obtained with the first oxygen neighbor removed is even closer to the experimental value observed, which also indicates this configuration as stable and present in the sample.

^{111}In(^{111}Cd): SnO_2 thin film

Figure 2(a) shows the TDPAC spectra measured at different temperatures using ^{111}In(^{111}Cd) as a probe nucleus implanted into SnO_2 thin films, including some of those already published in a previous work.[12] The data show a significant damping in the modulations of R(t) functions. Figure 2(b) shows the corresponding hyperfine parameters plotted as a function of the measuring temperature.

To help the discussion, the hyperfine parameters obtained for sites 1 and 2 are distinguished by EFG_1 and EFG_2, respectively.

In Table II, the hyperfine parameters of the thin films are displayed for each zone of possible electronic structures of the environment around the probe nuclei. By comparing our results with those from previous works,[8–14,25,26] we could associate the temperature dependence of the hyperfine parameters with different charge states, small indium oxide precipitates, and oxygen vacancies. For a comparison on the V_{zz} calculation, we used the old Q value of 0.83(13) b[27] although the most recent value is 0.683(20) b.[28]

Static quadrupole interactions of site 1

The EFG_1 yields smaller asymmetry parameters than EFG_2 in all the zones. Near room temperature, zone A, our results are in agreement with the *ab initio* calculations for a semi-charged rutile state. An increase in η in zones B and C was observed. This effect is probably due to very small In_2O_3 precipitates that did not fully achieve the complete structure of the oxide.[8] In addition, the values are similar to those in a particular case of In_2O_3 oxide, when oxygen vacancies in the neighborhood of Cd impurities are induced by the valence difference with respect to the cation, as previously reported for

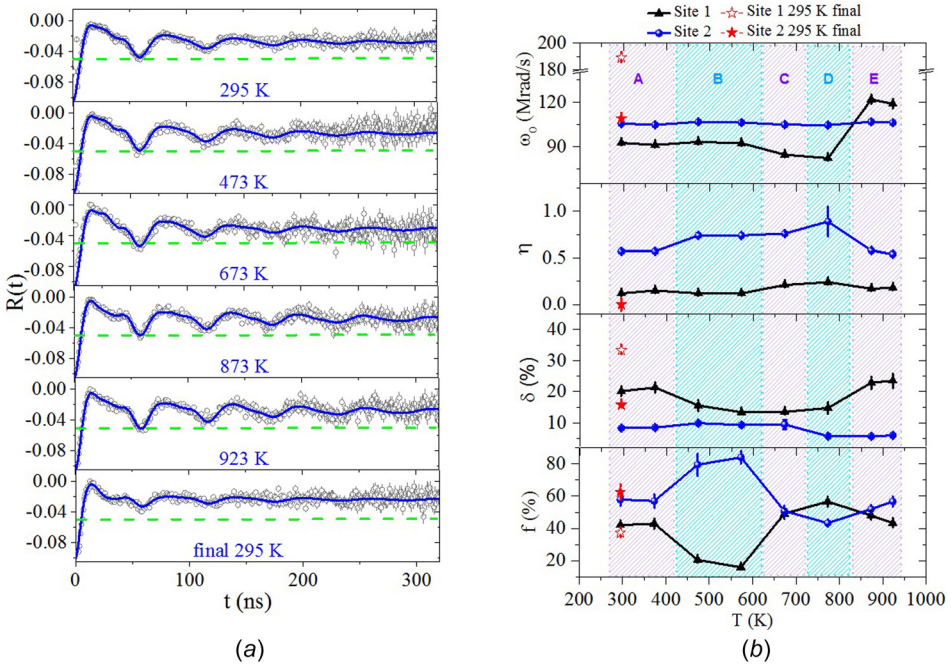

FIG. 2. (a) R(t) spectra obtained for the SnO_2 thin film using $^{111}In(^{111}Cd)$ after RTA. The three bottom spectra were previously published.[12] Dashed green lines are guides to the eye for $R(t) = -0.05$; (b) graphic representation of the corresponding hyperfine parameters as a function of temperature. Solid lines are guides to the eye, and the shaded rectangles define the zones of different states of rutile.

Cd impurities in In_2O_3 oxide, $V_{zz} = 5.83 \times 10^{21}$ V/m^2 and $\eta = 0.72$.[26] In zone D, the maximum η-value is observed, approaching both the values: for a relaxed rutile cell simulated using the Point Charge Model, PCM, and the experimental result at around 373 K.[25] Zone E is particular because the temperature achieved is equal to or higher than the one used for the RTA. The hyperfine parameters are close to the ones obtained in zone A. Since every measurement took 4–12 h, it is plausible to consider every step as a long thermal treatment. Specifically under nitrogen or in vacuum, it is likely that this affects the stoichiometry and/or resistivity of the films.[29] There are two zones, in which a fraction inversion takes place, zones C and E. The frequency distribution achieves its minimal value in zones B and C, and in general, EFG_1 presents higher δ values than EFG_2.

Static quadrupole interaction of site 2

The V_{zz} and η of EFG_2 in zones A and B are quite similar and can be compared to the charged state of rutile. In contrast, in zones C and D, the signal can be assigned as the neutral charge state.[25] Since the measurement temperatures in zone E are higher than those during the RTA, which precedes the measurements, this site presents the higher V_{zz} values. This can be seen as evidence of an oxygen diffusion process and is associated with the creation of several oxygen vacancies, resulting in a structural change in SnO.[9] Then, the local structure around the probes undergoes new reorganization during the several hour time scales of the TDPAC measurement.

The electric field gradient is very sensitive to the charge state of the probe nucleus neighborhood. ^{111}Cd and ^{117}In have different valence states (+2 and +3, respectively), which may result in different charge states when they act as dopants in SnO_2, where the cationic Sn has the valence state +4. Therefore, we expected different EFG measured values by these two probe nuclei, as observed in the experiments and confirmed by first-principles calculations. When a dopant has a smaller valence state than the resident cation in oxides, oxygen vacancies are possibly favored[26] particularly when the

TABLE II. Comparison of the experimentally and theoretically obtained hyperfine parameters for SnO_2.

		Experimental		Theory		
Zone	State	η	V_{zz} (10^{21} V/m^2)	η	V_{zz} (10^{21} V/m^2)	Reference
EFG_1						
A	Semi-charged	0.57 (2)	5.59	0.56	+5.93	25
B	In_2O_3 embryos	0.74 (3)	5.62	0.78(5)	5.39	8
C	In_2O_3 embryos	0.76 (2)	5.54	0.77(5)	5.27	8
D	Relaxed (PCM model)	0.89 (2)	5.53	0.95	−5.96	25
E	Semi-charged	0.54 (3)	5.62	0.56	+5.93	25
EFG_2						
A	Charged	0.15(1)	4.82	0.14	+5.47	25
B	Charged	0.12(1)	4.93	0.14	+5.47	25
C	Neutral	0.21(1)	4.47	0.26	+4.77	25
D	Neutral	0.24(1)	4.37	0.26	+4.77	25
E	New structural reorganization	0.18(1)	6.29			

annealing is carried out under a low pressure atmosphere. Furthermore, Cd needs an additional electric charge regarding In, and measurements are foreseen, in which ^{111}In is co-implanted with ^{111m}Cd by overheating the transfer line of the ISOLDE target.[30] This would allow us to study more closely the formation or trapping of defects such as oxygen vacancies as a function of the temperature.

CONCLUSION

For all the samples, the In/Cd atoms were located at substitutional Sn sites. Regarding applications, whether Cd/In substitutes Sn in the SnO_2 lattice is an important question and measurements of the electric field gradient via the TDPAC technique provided useful information as a function of temperature. In or Cd have lower charge and greater ionic radii than the host cation, causing a displacement of the coordinating O ions away from the Sn site center. Therefore, the sizes of the adjacent interstitial sites decrease. For ^{111}In, the effective annealing atmospheres were vacuum, but air in the case of ^{117}Cd. Even if that would play a role, decreasing oxygen vacancies and reducing the mobility of Cd atoms, the absence of strong damped spectra further indicates that implanted Cd atoms easily occupy regular substitutional Sn sites with good stability. This leaves open the possibility of achieving electrical doping via Cd/In ion implantation. But this is also a probable consequence of the careful control of the sample production and characterization of the doping method using diluted ppm concentrations of the probing atoms. The simulations performed with the ^{117}Cd probe near one oxygen vacancy show that when the vacancy is closer to the probe, the Vzz value is closer to the experimental value. Since there was no result with smaller Vzz, the second fraction remains unexplained.

The present work cannot answer all the observed phenomenology for the metallic Cd and In atoms in SnO_2, but it further presents the view of an ideally diluted method, TDPAC, providing clear results and systematics that can be refined upon new experiments to be performed under different annealing and sample composition conditions and morphologies. In this view, the technique opens interesting perspectives for studies on SnO_2 nanotubes and profits from the possibility of simultaneous ^{111}In and ^{111m}Cd implantation at ISOLDE.[30]

ACKNOWLEDGMENTS

The research leading to these results is related to the ISOLDE experiment LOI144 and has received funding from the European Union's Horizon 2020 research and innovation programme under grant agreement 654002, from the Federal Ministry of Education and Research, BMBF, through grants 05K13TSA and 05K16PGA, and from Fundação para a Ciência e a Tecnologia, FCT project CERN-FIS-NUC-0004-2015. In particular, J. Schell extends her thanks to the German Academic Exchange Service, DAAD, in collaboration with Conselho Nacional de Desenvolvimento Científico e Tecnológico, CNPq, through the fellowship Grant No. 290102/2011-1. We thank very much Ms. Noll and the BONIS team of the HISKP, Bonn, for the implantations and the warm hospitality. Dr. J. G. Martins Correia and the ISOLDE in-house group, in particular the RILIS team, are thankfully acknowledged for great discussions and technical support during the beam time.

[1]Ç. Kiliç and A. Zunger, Phys. Rev. Lett. **88**, 095501 (2002).
[2]L. Wang, J. Li, Y. Wang, K. Yu, X. Tang, Y. Zhang, S. Wang, and C. Wei, Nat. Sci. Rep. **6**, 35079 (2016).
[3]M. Liu, Y. Liu, Y. Zhang, Y. Li, P. Zhang, Y. Yan, and T. Liu, Nat. Sci. Rep. **6**, 31496 (2016).
[4]Z. Tianshu, P. Hing, Y. Li, and Z. Jiancheng, Sens. Actuators, B **60**, 208 (1999).
[5]P. Sun, X. Zhou, C. Wang, B. Wang, X. Xu, and G. Lu, Sens. Actuators, B **190**, 32 (2014).
[6]E. Mark, O. B. White, M.-Y. Tsai, and S. S. James, Appl. Phys. Express **3**, 051101 (2010).
[7]S. Sujatha Lekshmy and K. Joy, J. Mater. Sci.: Mater. Electron. **25**, 1664 (2014).
[8]J. Desimoni, A. G. Bibiloni, L. A. Mendoza-Zélis, L. C. Damonte, F. H. Sanchez, and A. Lopez, Garcia, Hyperfine Interact. **34**, 271 (1987).
[9]M. Renteria, A. G. Bibiloni, M. S. Moreno, J. Desimoni, R. C. Mercader, A. Bartos, M. Uhrmacher, and K. P. Lieb, J. Phys.: Condens. Matter **3**, 3625 (1991).
[10]H. Wolf, S. Deubler, D. Forkel, H. Foettinger, M. Iwatschenko-Borho, M. Meyer, M. Rem, and W. Witthuhn, Mater. Sci. Forum **10–12**, 863 (1986).
[11]J. M. Ramos, A. W. Carbonari, M. S. Costa, and R. N. Saxena, Hyperfine Interact. **197**, 239 (2010).
[12]J. M. Ramos, T. Martucci, A. W. Carbonari, M. S. Costa, R. N. Saxena, and R. Vianden, Hyperfine Interact. **221**, 129 (2013).
[13]E. L. Muñoz, A. W. Carbonari, L. A. Errico, A. G. Bibiloni, H. Petrilli, and M. Renteria, Hyperfine Interactions **178**, 37 (2007).
[14]J. Schell, "Investigation of hyperfine parameters in Pure and 3d transition metal doped SnO_2 and TiO_2 by means of perturbed gamma-gamma angular correlation spectroscopy," Ph.D. thesis (São Paulo University, Brazil, 2015).
[15]A. Abragam and R. V. Pound, Phys. Rev. **92**, 943 (1953).
[16]H. Frauenfelder, R. M. Steffen, and K. Siegbahn, in *α-, β- and γ-Ray Spectroscopy*, edited by K. Siegbahn (North-Holland, Amsterdam, 1965), Chap. XIX.
[17]E. Kugler, Hyperfine Interact. **129**, 23 (2000).
[18]S. Rothe, T. D. Goodacre, D. V. Fedorov, V. N. Fedosseev, B. A. Marsh, P. L. Molkanov, R. E. Rossel, M. D. Seliverstov, M. Veinhard, and K. D. A. Wendt, Nucl. Instrum. Methods Phys. Res. Sect. B **376**, 91 (2016).
[19]M. A. Nagl, M. B. Barbosa, U. Vetter, J. G. Correia, and H. C. Hofsäss, Nucl. Instrum. Methods Phys. Res. Sect. A **726**, 17 (2013).
[20]P. Blaha, K. Schwarz, G. K. H. Madsen, D. Kvasnicka, and J. Luitz, *WIEN2K: An Augmented Plane Wave+Local Orbitals Program for Calculating Crystal Properties* (Karlheinz Schwarz, Technische Universität, Wien, Austria, 1999).
[21]P. E. Blöchl, Phys. Rev. B **50**, 17953 (1994).
[22]G. Kresse and J. Furthmüller, Phys. Rev. B **54**, 11169 (1996).
[23]A. A. Bolzan, C. Fong, B. J. Kennedy, and C. J. Howard, Acta Crystallogr. B **53**, 373 (1997).
[24]P. Perdew, K. Burke, and M. Ernzerhof, Phys. Rev. Lett. **77**, 3865 (1996).
[25]E. L. Muñoz, Ph.D. thesis, Universidad Nacional de La Plata, Argentina, 2011.
[26]C. Sena, M. S. Costa, E. L. Muñoz, G. A. Cabrera-Pasca, L. F. D. Pereira, J. Mestnik-Filho, A. W. Carbonari, and J. A. H. Coaquira, J. Magn. Magn. Mater. **387**, 165 (2015).
[27]P. Herzog, K. Freitag, M. Reuschenbach, and H. Walitzki, Z. Phys. A: At. Nucl. **294**, 13 (1980).
[28]H. Haas, M. B. Barbosa, and J. G. Correia, Hyperfine Interact. **237**, 115 (2016).
[29]K. B. Sundaram and G. K. Bhagavat, J. Phys. D: Appl. Phys. **16**, 69 (1983).
[30]J. Schell, D. C. Lupascu, J. G. M. Correia, A. W. Carbonari, M. Deicher, M. B. Barbosa, R. D. Mansano, K. Johnston, I. S. Ribeiro, Jr., and ISOLDE Collaboration, Hyperfine Interact. **238**, 2 (2017).